HHS Public Access

Author manuscript

Biomaterials. Author manuscript; available in PMC 2017 May 01.

Published in final edited form as:

Biomaterials. 2016 May ; 87: 157–169. doi:10.1016/j.biomaterials.2016.02.013.

Dexamethasone retrodialysis attenuates microglial response to implanted probes *in vivo*

Takashi D.Y. Kozai[1,2,3,4], **Andrea S Jaquins-Gerstl**[5], **Alberto L Vazquez**[1,2,6], **Adrian C Michael**[5], and **X. Tracy Cui**[1,2,3]

[1]Bioengineering, University of Pittsburgh

[2]Center for the Neural Basis of Cognition

[3]McGowan Institute for Regenerative Medicine, University of Pittsburgh

[4]Neurotech Center of the University of Pittsburgh Brain Institute

[5]Chemistry, University of Pittsburgh

[6]Radiology, University of Pittsburgh

Abstract

Intracortical neural probes enable researchers to measure electrical and chemical signals in the brain. However, penetration injury from probe insertion into living brain tissue leads to an inflammatory tissue response. In turn, microglia are activated, which leads to encapsulation of the probe and release of pro-inflammatory cytokines. This inflammatory tissue response alters the electrical and chemical microenvironment surrounding the implanted probe, which may in turn interfere with signal acquisition. Dexamethasone (Dex), a potent anti-inflammatory steroid, can be used to prevent and diminish tissue disruptions caused by probe implantation. Herein, we report retrodialysis administration of dexamethasone while using *in vivo* two-photon microscopy to observe real-time microglial reaction to the implanted probe. Microdialysis probes under artificial cerebrospinal fluid (aCSF) perfusion with or without Dex were implanted into the cortex of transgenic mice that express GFP in microglia under the CX3CR1 promoter and imaged for 6 hours. Acute morphological changes in microglia were evident around the microdialysis probe. The radius of microglia activation was 177.1 μm with aCSF control compared to 93.0 μm with Dex perfusion. T-stage morphology and microglia directionality indices were also used to quantify the microglial response to implanted probes as a function of distance. Dexamethasone had a profound effect on the microglia morphology and reduced the acute activation of these cells.

Corresponding authors: Takashi D.Y. Kozai, Ph.D., Department of Bioengineering, University of Pittsburgh, 208 Center for Bioengineering, 300 Technology Drive, Pittsburgh, PA 15219, Ph: 412-383-9044, tdk18@pitt.edu. X. Tracy Cui, Ph.D., Department of Bioengineering, University of Pittsburgh, 5057 Biomedical Science Tower 3, 3501 Fifth Avenue, Pittsburgh, PA 15260, Ph: 412-383-6672, Fx: 412-648-9076, xic11@pitt.edu.

Keywords

Microglia; Microdialysis; Multiphoton Microscopy; Dexamethasone; Brain Penetration-injury; Blood-Brain Barrier (BBB)

INTRODUCTION

Implantable neural probes are powerful tools for understanding brain function as well as a critical front-end system for monitoring brain physiology, especially in the clinical setting [1–10]. The use of probes to monitor neurotransmitters and neurochemicals has led to significant advances in understanding the brain's physiology and neurochemistry in mental health disorders, neurolological disease, and brain injury [11–21]. Among various neural probes for *in vivo* biochemical sensing, brain microdialysis probes present a major advantage in that they are not limited to electroactive species and can be combined with analytical techniques that can more easily separate multiple neurochemical targets of interest from interferents [22]. However, there are challenges in reliable sampling from implanted microdialysis probes [23–29].

Implantation of neural probe devices into the brain results in immediate tissue injury and blood-brain barrier (BBB) disruption [30–32], activation of microglia and astrocytes [32, 33], inflammation [34], loss of oxygen perfusion [22, 32, 33] and neural degeneration. These reactive tissue responses have been extensively characterized for smaller electrophysiology electrodes, which are sensitive to small ionic currents from action potentials (see review [4, 32]). One cell type that plays a critical role after device implantation is microglia. Microglia normally perform a wide range of tasks while in the native ramified (R-stage) state, including experience-dependent synaptic maintenance [35, 36], debris clearing [37], and surveillance against injury and invasion [37]. Acutely, following probe insertion, nearby microglia activate and encapsulate the implant with their processes and lamellipodia sheath [33]. A previous *in vivo* two-photon study showed that nearby microglia enter a transition stage (T-stage) where microglia retract most of their processes while extending a few long processes towards the implant on the order of minutes [33] in a manner similar to the microglia response to BBB injury by laser ablation [33, 38]. During the first 12 hours once these processes reach the surface of the probe, very little morphological change is observed [33]. Over days and weeks, the microglia migrate to the surface of the implant and form a thin cellular sheath that encapsulates the device [39, 40]. Microglial activation is also accompanied by activation of astrocytes, often characterized by glial fibrillary acid protein upregulation [34, 41–44]. The glial sheath in turn forms a barrier that impedes ionic current and neurochemical diffusion [45]. In addition, caspase-1 mediates neuronal loss, and a decrease in neurite density has been found which alters the sampling environment around implanted devices [27, 28, 34, 46–48]. This leads to a degradation of electrical and electrochemical signal quality over the lifetime of the implant [1, 28, 34, 44, 49, 50].

Numerous intervention strategies to minimize the inflammatory tissue responses to neural implants have been proposed and/or investigated including device footprint size [44, 51, 52], electrode site size [44, 53], volumetric density across the device's footprint [54, 55], strength

[44, 56], compliance/flexibility [44, 57], elasticity/softness [58–61], electrical properties [62–66], device insertion speed [67, 68], tip shape[67], surface modifications [44, 69–71 and 109], and drug delivery [27–29, 72–79]. In particular, dexamethasone (Dex), an anti-inflammatory synthetic glucocorticoid, has been frequently used to reduce inflammation and the reactive tissue response around surgical implants [80, 81], and more recently for use with brain implants [27–29, 72–79, 82]. In particular, microdialysis studies have shown that continuous retrodialysis of Dex mitigates ischemia and gliosis and also reduces activation of microglia at 4 and 24 hours based on postmortem histology [28, 29]. Longer term studies demonstrated that retrodialysis of Dex for 5 days was highly effective at suppressing the formation of a glial scar at the probe track and significantly reduced the presences of microglia [27] [108]. The actions of Dex are anti-inflammatory and are tightly confined to the local vicinity of the microdialysis probes. Dex does not distort neurochemical measurements, and the tissues surrounding implants are stable and robust [27–29]. Although Dex administration reduces the extent of inflammatory gliosis, it is uncertain how its action affects microglia morphology/motility in real time. Characterizing the dynamic microglia response to penetration of microdialysis probes and the Dex treatment will shed light towards the understanding of the brain penetration injury and mechanism of action of anti-inflammatory therapeutics.

In previous studies, ED-1 labeling in the presence of Dex did not show significant microglial activation at the 4-hour time point following microdialysis probe insertion [27–29]. Therefore, the dynamics of interest for this study are over the acute time period. Here we employ *in vivo* two-photon microscopy to quantify the acute microglial response to microdialysis probes in brain with or without retrodialysis of Dex. Specifically, we examine the cellular microglial response to microdialysis probe insertion until 6 hours post-implantation while infusing either artificial cerebral spinal fluid (aCSF) or Dex. Morphological changes and activation characteristics of microglia around the implants were observed and quantified.

MATERIALS and METHODS

Microdialysis Probe and Perfusion Preparation

Vertical concentric microdialysis probes (300 μm o.d., 4mm in length) were constructed with a hollow fiber dialysis membrane (Spectra-Por RC Hollow Fiber; MWCO: 13,000 Da, 300 μm o.d., 160 μm i.d., Spectrum Laboratories, Inc.; Rancho Dominguez, CA) and fused silica outlet lines (150 μm o.d., 75 μm i.d., Polymicro Technologies; Phoenix, AZ) as described elsewhere [83]. Artificial cerebrospinal fluid (aCSF: 142 mM NaCl, 1.2 mM $CaCl_2$, 2.7 mM KCl, 1.0 mM $MgCl_2$, 2.0 mM NaH_2PO_4, pH 7.4) was the perfusion fluid in control experiments. Dexamethasone sodium phosphate (Dex, APP Pharmaceuticals LLC Schaumburg, Il) was diluted in aCSF to 10 μM.

Surgery

Microdialysis probes were bilaterally implanted in cortex area V1/V2 of ten transgenic mice that express green fluorescent protein (GFP) in brain microglia under the direction of the CX3CR1 promoter (CX3CR1-GFP). CX3CR1-GFP mice were obtained from Jackson

Laboratories (Bar Harbor, ME) and weighed 25–30 g. These animals were prepared for cortical implants using previously established methods [30, 33]. Briefly, the animals were anesthetized with a mixture of 90 mg kg−1 ketamine and 9mg kg−1 xylazine administered intraperitoneally (IP) with regular updates of 17.5 mg kg−1 every hour or as needed. The depth of anesthesia was monitored by tracking heart rate. After the animal was placed in a stereotaxic frame, the skin and connective tissue on the surface of the skull was removed. A thin layer of Vetbond (3M) was placed over the skull and a 1–1.5 mm tall well was constructed around the edges of the skull using dental cement. A 4 mm by 6 mm craniotomy was made by thinning the skull over the somatosensory and visual cortex using a high-speed dental drill and then removed with forceps. The skull was periodically bathed in saline to ensure that the underlying cortex did not experience thermal damage from drilling. Care was taken to prevent vascular damage during drilling and the removal of the bone. All experimental protocols were approved by the University of Pittsburgh, Division of Laboratory Animal Resources and Institutional Animal Care and Use Committee in accordance with the standards for humane animal care as set by the Animal Welfare Act and the National Institutes of Health Guide for the Care and Use of Laboratory Animals.

Probe Insertion

The microdialysis probes were aligned with a stereotaxic manipulator over the visual cortex at a 30° angle. Prior to insertion, probes were continuously perfused with artificial cerebrospinal fluid (aCSF: 144 mM Na^+, 1.2 mM Ca^{2+}, 2.7 mM K^+, 152 mM Cl^-, 1.0 mM Mg^{2+}, and 2.0 M PO_4^{3-} adjusted to pH 7.4 with NaOH) or 10 μM Dexamethasone in aCSF at 0.610 μL/min until the conclusion of the experiment. Flow was confirmed by visual inspection of droplets forming at the outlet line but samples were not collected for analysis. Probes were inserted using a z-axis automated microdrive (MO-81, Narishige, Japan) at 200 μm s−1 for 2700 μm, then retracted 300 μm. Probes were then fixed into position using a blue-light curing dental cement. Then, prior to imaging, 0.1 cc of 1 mg ml−1 sulforhodamine101 (SR101, S-359, Invitrogen, Carlsbad, CA) was injected IV as an optical vascular label (red), and then 0.05 mg ml−1 SR101 was administered IP periodically as needed as the blood vessels became faintly labeled.

Two-photon imaging

A two-photon laser scanning microscope was used for *in vivo* imaging. The microscope consisted of a scan head (Bruker/Prairie Technologies, Madison, WI) and a Ti:sapphire laser (Mai Tai DS; Spectra-Physics, Menlo Park, CA) providing 100 fs pulses at 80 MHz tuned at a wavelength of 920 nm for this study. A 16×, 0.8 numerical aperture water immersion objective lens was used for imaging (Nikon Instruments Inc., Melville, NY). Fluorescence was detected using non-descanned photomultiplier tubes (Hamamatsu Photonics KK, Hamamatsu, Shizuoka, Japan) in whole-field detection mode. Images of 1024 × 1024 pixel (815 μm × 815 μm) were acquired using Prairie View software. Z-stacks were taken every hour with 2 μm step-size.

Data Analysis

Because the microdialysis probes needed to be fixed onto the headcap prior to imaging, the earliest z-stack time point was 0.5 hr post implant. In a previous publication with solid

silicon implants, the initial microglia response settled within the 1st hour and then showed limited morphological change over the first 6 hrs [33]. In some previous animals, anesthesia related issues caused deterioration of the animal health and tissue around 7–8 hrs post implant [33]. Therefore, quantitative morphological analysis was conducted at the 6 hr time point [33]. Microglial cells were characterized as ramified or in the activated transitional stage (T-stage), characterized by retraction of most processes with extension of others toward the insult or injury location. The number of ramified cells divided by total cells were then binned by distances and averaged across trials to generate p, the probability that a microglia body will be in the ramified state in each bin. Because the p with respect to distance plot follows a Bernoulli distribution, a binomial logarithmic generalized linear regression was used to deduce the distance for a given p:

$$\log\left(\frac{p}{1-p}\right)=\alpha+\beta x \quad [1]$$

where p represents the ramification index, and x represents the distance from the probe as previously established [33].

Measurements and calculation of a T-stage morphology index and microglia directionality index was also performed to assess the activated state of microglia by two counters. T-stage morphology index was calculated by measuring the length (n) of the longest microglia process from the hemisphere facing the probe and the length (f) of the longest process facing away from the probe at 6 hr post implantation. Similarly, microglia directionality index was calculated by measuring the number of processes (n) extending from the cell body in the hemisphere facing the probe and the number of processes (f) extending from the cell body in the hemisphere facing away from the probe. Index values were calculated using the following formula as previously established [33]:

$$Index=\frac{(f-n)}{(f+n)}+1 \quad [2]$$

In both cases, an index value of 1 represents a ramified microglia cell ($n=f$), while an index of 0 represents a fully active T-stage microglia cell extending all processes toward the implant, similar to the microglia ramification state rating method. Note that if a microglia reduces 'f' by 50% and increases 'n' by 50%, the resulting index will be 0.5. Binning was performed to compute error bars as a function of distance for the indices, and the size of each bin was 30 μm. The distribution of the index values as a function of cell body distance from the implant was then generated. This distribution was fitted to a dual sigmoidal function as done previously using a custom MATLAB script [33]. This function was used to capture the plateau feature between normal ramified microglia and T-stage active microglia, which corresponds to 1 and 0, respectively. The sigmoidal function was parameterized by amplitude (a), shoulder location (d_1 and d_2 in μm), and shoulder width (w_1 and w_2 in μm) and the fit was constrained to indexes between 0 and 1 (Eqn. [3]). To determine the distance where the microglia morphology differs from a non-active microglia, the data were binned over 30μm increments and mean and standard deviation of the index values were computed. Welsh t-tests were computed over each bin and significant differences were established for

p<0.05. In addition, chi-squared values and two-sided t-tests of the residuals were used to evaluate the model adequacy relative to a simple linear model as previously established [33].

$$y(d)=\frac{a}{1+e^{-(d-d_1)/w_1}}+\frac{1-a}{1+e^{-(d-d_2)/w_2}} \quad [3]$$

3D reconstruction

To qualitatively capture the response of microglia to the implant, high-resolution stacks were reconstructed into three-dimensional space by linear interpolation. In some cases, the reconstructed volume was rotated for visualization. This was performed using ImageJ's (NIH) built-in '3D Project' function. Visualization of microglia activity adjacent to the implant was done by setting the function's interior depth-cueing parameter to zero. An average intensity projection was then performed parallel and perpendicular to the electrode penetration orientations.

RESULTS

As previously established, care was taken to prevent vascular damage during drilling and removal of the bone [30, 33]. Microdialysis probes were inserted with the beveled tip facing up over an area of the cortex with relatively low vessel density (usually between areas V2 and S1) as shown in Figs.1 and 2. Microglial cells were continuously monitored over a 6 hr period; representative images are shown in Fig. 1 (d–h). Due to the size of the microdialysis probes, bleeding was sometimes observed during insertion. In these cases, regions of the tissue unobscured by blood were quantified. Laser and PMT settings were sometimes increased within safety limits before re-imaging bloody tissue regions (which caused other regions of the tissue to saturate the detectors). Continuous retrodialysis of 10 μM dexamethasone in aCSF at 0.610 μL/min altered the microglial activation pattern when compared to aCSF only perfusion. Fig. 2 illustrates a microdialysis probe inserted into the cortex while both microglial cells (green) and the vasculature (red) were monitored. 3D projection images are shown from a side view (Fig. 2 b) and from the top (Fig. 2 c). These images helped characterize and visualize the morphology and directionality of the microglia in the presences of Dex or aCSF.

Microglia activation radius at 6 hours

Microglia cells reacted immediately following probe insertion into the cortex. In order to quantify microglia activation and correlate it to the distance to the probe, microglia cells were assigned a binary score: 0 for activated and 1 for ramified. Then, a logarithmic binomial generalized linear regression curve was fitted to these data (Eq. [1]). At 6 hours post-insertion with aCSF, the probability of microglia being active was 50% (p=0.5) at a distance of 177.1μm (β=0.0293, α=5.189; Fig. 3). In contrast, the distance to a 50% probability for active microglia with Dex was reduced to 93.0μm (β=0.0319, α=2.966; Fig. 3), suggesting that Dex reduced the extent of active microglia.

T-stage morphology index

The T-stage activation of microglia cells was quantified as an index value following Eq. 1. (An index value of 1 represents ramified cells, while an index value of 0 represents fully activated microglia.) These index values were plotted as a function of distance from the probe for aCSF perfused (Fig. 4a) and Dex perfused (Fig. 4b) brain tissue. Note that the average index values for all bins were larger for the Dex data compared to the aCSF data, indicating that under Dex the microglia were less reactive than under aCSF perfusate. A two-shoulder function was used to characterize this distribution with the following parameter values: relative amplitude (a), near shoulder (d1) and spread (w1), and far shoulder (d2) and spread (w2) (Fig. 4c). For aCSF, a=0.77, d1=142 μm, w1= 164 μm, d2 = 177, w2 = 13 μm. In contrast for Dex, a=0.86, d1=22 μm, w1=21 μm, d2=180 μm, w2=2 μm. Welch's t-tests were performed on the index data from each bin between aCSF and Dex perfused microdialysis probes. Significant differences were observed in the 5 bins between 30 μm and 210 μm from the probe surface. Goodness-of-fit (chi-squared) metrics were calculated to ensure the model is appropriate. Chi-squared values of 3.9 and 14.4 were obtained for the Dex and aCSF data, respectively, which indicate that the model is not over fitting the binned data. In addition, we performed t-tests on the residuals of the model to ensure that the two-shoulder model is more appropriate to describe the data compared to a simple linear model. Both chi-squared metrics and t-tests showed that the two-shoulder model better described the Dex data (chi-sq=3.9, t-test $p<0.0001$) compared to a linear model (chi-sq=27.6, $p<0.01$) but a linear model performed similarly for the aCSF binned data (two-shoulder model chi-sq=14.4, $p<0.0001$; linear model chi-sq=19.5, $p<0.0001$). This finding is not surprising given the behavior of the relatively slow transition of the aCSF data with distance in Figure 4. Nonetheless, we report two-shoulder model parameter estimates for aCSF and Dex data for consistency and comparison.

Microglia directionality index

The directional preference of microglia's processes was quantified as an index value following Eq. 1. (An index value of 1 represents ramified cells, while an index value of 0 represents fully activated microglia.) These index values were plotted as a function of distance from the probe for aCSF perfused (Fig. 5a) and Dex perfused (Fig. 5b) brain tissue. As before, the average index values for all bins were larger for the Dex data except the first bin compared to the aCSF data; indicating that under Dex the microglia were less reactive than under aCSF perfusate. The two-shoulder function was then used to characterize this distribution with the following parameter values: relative amplitude (a), near shoulder (d1) and spread (w1), and far shoulder (d2) and spread (w2) (Fig. 5c). For aCSF, a=0.42, d1=1 μm, w1= 8 μm, d2 = 151, w2 = 62 μm. In contrast for Dex, a=0.81, d1=18 μm, w1=22 μm, d2=108 μm, w2=5 μm. Welch's t-tests were performed on the index data from each bin between aCSF and Dex perfused microdialysis probes. Significant differences were observed in the 3 bins between 90 μm and 210 μm from the probe surface. The two-shoulder model was well-suited to describe the aCSF data (chi-sq=10.9, $p<0.0001$) compared to a linear model (chi-sq=63.2, $p<0.001$), but the linear model performed similarly to the two-shoulder model for the aCSF data (two-shoulder chi-sq=6.8, $p<0.0001$; linear model chi-sq=7.4, $p<0.0001$). Nonetheless, the two-shoulder model was able to describe the data and the parameter estimates were used for comparison.

Microglia morphological differences between 1 to 6 hrs post-implantation

While the images acquired prior to 6-hours post-implantation were not analyzed as in Figures 3–5, the evolution of the tissue response shows different features depending on the perfusate. Microglia with cell bodies that were ~70–100 μm from the surface of aCSF perfused microdialysis probe were activated and polarized towards the microdialysis probe as expected within 30 minutes post implantation. An unexpected finding was that in all aCSF implants the microglia further from the probe (100–200 μm) generally retracted their processes over the first 2 hr (Fig. 6). From 2 hr the cells gradually increased thin basal processes in a manner consistent with polarization in the general direction of the implant. In a small number of exceptions, processes extended towards nearby BBB structures as previously shown [33].

In contrast, Dex perfusing microdialysis probes experience a much more limited response. In general, microglia that are activated and polarized at 30 min remain activated and polarized at 6 hr, while microglia that have radially extended processes at 30 min maintain radially projected processes at 6 hrs. As with ramified microglia, the processes continue to move surveying the nearby tissue [33]. One notable difference from ramified processes and the thin basal processes near aCSF perfusion probes is that the processes around Dex perfused probes gradually increase the thickness of their processes and increase the number of thick apical processes (Fig 7a). In one situation, microglia around a Dex perfused microdialysis probe demonstrated a reduction in processes over the first two hours, and then generally did not project new processes over the remaining 6 hours (Fig. 7b). The few processes that these cells had were short and thick. While Dex generally decreased microglial activation, some unusual morphologies were occasionally detected.

At 6 hr post-implant, microglia around aCSF perfused microdialysis probes had largely retracted most of their processes (Fig. 8bc, 9b), compared to normal microglia at the same depth [far away from the probe] (Fig. 8a, 9a). In contrast at 6 hr post-implant around Dex perfused microdialysis probes, microglia cells generally had processes that were radially projected (Fig. 8d, 9c). However, these processes appear to be thicker than ramified microglia and had greater apical processes. In one case, the microglia around a Dex microdialysis probe had retracted most of their processes and were generally wrapped around BBB structures (Fig 8e, 9d). This activation pattern was unrelated to Dex concentration, perfusion speed, or inter-animal variability as Figure 8d and Figure 8e were tissue reactions from opposite sides of the same probe in the same animal and implant location. Careful anatomical and blood flow examination revealed that there was a large arteriole on the side of 6d. This arteriole may have also perfused into the tissue region of 6e, but was separated by the microdialysis probe due to insertion. Additional research is necessary to understand if arterial supply and metabolics are associated with this large difference in microglia reaction (Fig. 8de, 9cd).

Discussion

Dex is a popular anti-inflammatory drug. It is a synthetic glucocorticoid or corticosteroid which binds more tightly to the Glucocorticoid Receptor than cortisol, a natural glucocorticoid synthesized in the adrenal cortex [84]. Cortisol activates a feedback

mechanism that upregulates anti-inflammatory proteins, and transrepresses proinflammatory transcription factors from entering the nucleus [85]. Furthermore, glucocorticoid receptors are expressed in most cells including microglia [86]. These properties have made Dex a popular drug to reduce inflammation in a variety of inflammatory diseases and following non-brain related surgery [87–93]. Although frequently studied for neural inflammation, its direct effect on microglia activation, particularly motility and morphology has not been characterized prior to this study.

Radius of microglia activation at 6 hr

In a previous publication, we demonstrated that microglial cells immediately reacted to relatively small probes (15 μm × 55 μm) inserted into the cortex [33]. In order to quantify and correlate the probability of microglia activation with respect to the distance to the probe, a logarithmic binomial generalized linear regression curve was fitted to the distribution (Eq. [1]). At 6 hours post-insertion, the probability of microglia being active was 50% (p=0.5 in Eq. 3) within a distance (Eq. 3) of 130.0 μm from the probe (β=0.0587, α=−7.630 in Eq. 3):

$$\log\left(\frac{p}{1-p}\right)=0.0587x-7.63$$

In contrast, aCSF perfused 300 μm diameter had a p=0.5 value at a distance of 177.1 μm (Fig. 3):

$$\log\left(\frac{p}{1-p}\right)=0..0293x-5.189$$

The increased p=0.5 may, in part, be due to the increased size of the microdialysis probes. When perfused with dexamethasone, the p=0.5 value decreased to 93.0 μm (Fig. 3):

$$\log\left(\frac{p}{1-p}\right)=0.0319x-2.966$$

suggesting that the dexamethasone reduced the activation radius of nearby microglia.

Temporal dynamics of microglial response

In all aCSF implants the microglia further from the probe (100–200 μm) generally retracted their processes over the first 2 hr (Fig. 6), but then gradually increased thin basal processes in a manner consistent with polarization towards the implant. In contrast, tissue around Dex perfusing probes experience a much more limited dynamic response between 30 min and 6 hrs. When compared to silicon microelectrodes an important difference was that the silicon does not have a porous surface. However, this alone does not explain the general process retraction that occurs at 2 hrs.

Another important difference is that the cross-sectional surface area of each silicon shank of the microelectrode was roughly 825 μm^2 compared to the 70,800 μm^2 of the microdialysis probe. The ~90 times increased volume of the implant means much more tissue needs to be

displaced to accommodate the probe. In turn, this means more tissue strain is experienced by the nearby tissue compared to smaller silicon microelectrodes or carbon fiber implants [34]. It is possible that the increased tissue strain leads to increased intracellular pressure and negatively impacted normal protein function [94, 95]. Chaperone proteins may respond by retracting processes to prevent rupture or tear of processes and maintain lipid membrane integrity [96, 97]. Once the pressure equilibrates, at least to some threshold, the cells can resume normal function and polarize towards the injury. However, the exact mechanisms and their contributions to this dynamic tissue response still need to be studied.

Large microglia morphological differences induced by Dex

Postmortem histological studies have shown that Dex restored blood flow, diminished ischemia, minimized neuronal loss, reduced the appearance of extravagated macrophages and suppressed gliosis near microdialysis probes implanted in the rat striatum [29]. Furthermore, Dex significantly attenuated the loss of dopamine activity in the tissue next to the microdialysis probes. Studies such as these confirmed the ability of Dex to mitigate the effects of the penetration injury caused by microdialysis probes [22, 28, 29]. Although these steroids such as Dex inhibited the production of pro-inflammatory factors, side effects do occur [98–101]. Many of these side effects, such as indigestion, were due to systemic administration. In contrast, the local administration of Dex rendered it a great candidate to reduce the effects of penetration injury by neural probes.

Figures 7a and 7b, 8d and 8e, as well as 9c and 9d showed that Dex can cause large differences in microglial morphology that were not necessarily captured by traditional microglia activation metrics. While most microglia cells generally had processes that were radially projected (Fig. 7a, 8d, 9c), in some instances the microglia around Dex microdialysis probes had retracted most of their processes in a near amoeboid morphology and were generally wrapped around nearby BBB structures (Fig 7b, 8e, 9d). Beyond the role of Dex as an anti-inflammatory drug, glucocorticoids have important roles regulating metabolic, arousal, attention, cardiovascular, and homeostatic functions [102–104]. The Dex related changes in metabolism may contribute to the thickening of processes and increased apical processes compared to ramified microglia, although this remains to be studied (Fig. 9a&c). Previous research has shown loss of perfusion and evidence of ischemia around the implants [33, 34, 105]. When vascular injury during probe insertion is limited, Dex may be neuroprotective due to its anti-inflammatory effect. In contrast, if key vascular structures are damaged during probe insertion, delivery of oxygen and nutrients (and removal of neurotoxic waste products) may be reduced [32], and Dex might exacerbate local ischemia due its associated changes in cellular metabolic rate. Additional research should examine if these opposing effects of Dex, suppression of inflammation and changes in cellular metabolism, contribute to the large difference in microglia response observed in our data.

In order to study if the combination of increased metabolic consumption due to Dex and decreased metabolic supply from accidentally damaging arterioles may lead to greater metabolic disparity and the associated glial response to nearby BBB, careful anatomical and blood flow examination is necessary. Examination of our data revealed that there was a large arteriole on the side of 8d. This arteriole may have also perfused blood flow into the tissue

region of 8e, but was separated by the microdialysis probe during to insertion. In turn, this may have led to reduced oxygen perfusion and metabolic supply to the corresponding tissue (Fig. 8e). One possibility is that microglia in Figure 8d appear largely ramified due to the maintained proximity to the arteriole. In contrast in Figure 8e, the combination of reduced oxygen perfusion from steric separation of the nearest arteriole and increase in metabolic consumption may have led to their retraction of processes and encapsulation of the nearby blood vessel (capillaries and venuoles). Future research should examine the impact of altering arterial vs. venous blood flow on microglia activation around microdialysis probes perfused with Dex and aCSF. Arteries and veins can be easily differentiated in the cortex by blood flow direction, transgenic labels such as smooth muscle actin (Fig. 10), and morphology (Fig. 11). Arterial flow blockage disrupts mostly downstream perfusion while venous flow blockage shows significant upstream effects (stagnation). A more controlled study is necessary in order to understand the non-uniform microglia injury response patterns in the presence of Dex (Fig. 7a&b, 8d&e, 9c&d). Understanding the specific contribution of artery and vein injury on electrophysiology recording performance and sensitivity of electrochemical sensors over time may also be a key step in understanding the larger inter-animal and intra-animal variability often reported in the literature [30, 106, 107].

CONCLUSION

This work leads to several significant findings regarding acute microglia response to microdialysis probe implantation and effect of retrodialysis of Dex. Implantation of the microdialysis probe and aCSF perfusion elicited a delayed but larger activation of microglia compared to previously studied microelectrode implants. Dex had a significant effect on the radius of microglia activation, morphology, T-stage activation of microglia cells, and microglia directionality index. The temporal dynamics of microglial response also showed distinct differences between the aCSF control and Dex treated tissue. While many microglia appeared non-polarized with unusually thicker processes in the Dex treated tissue at 6 hr, some polarized towards nearby BBB. Such non-uniform microglia morphological response to Dex highlights the complexity of Dex's action in the heterogeneous brain tissue-implant environment. Real-time live animal imaging enabled us to take an in-depth look at the immediate and complex cellular response with high temporal and spatial accuracy. It will be of great interest in the future to examine the effect of Dex and other therapeutic candidates on penetration injury associated with brain tissue using longitudinal imaging techniques [40].

Acknowledgments

This project was financially supported by NIH R01 (Grant 5R01NS062019, 1R01NS089688, and 1R01NS094396-01), NIH R21 (GrantNS086107), and NIH K01 (Grant 1K01NS066131). The authors will like to thank Gregory Brunette for assistance with T-index quantification.

References

1. Kozai TDY, Du Z, Gugel ZV, Smith MA, Chase SM, Bodily LM, et al. Comprehensive chronic laminar single-unit, multi-unit, and local field potential recording performance with planar single shank electrode arrays. Journal of Neuroscience Methods. 2015; 242:15–40. [PubMed: 25542351]

2. Kozai TDY, Vazquez AL. Photoelectric artefact from optogenetics and imaging on microelectrodes and bioelectronics: New Challenges and Opportunities. Journal of Materials Chemistry B. 2015; 3:4965–78.

3. Kozai, T.; Alba, N.; Zhang, H.; Kotov, N.; Gaunt, R.; Cui, X. Nanostructured Coatings for Improved Charge Delivery to Neurons. In: Vittorio, MD.; Martiradonna, L.; Assad, J., editors. Nanotechnology and Neuroscience: Nano-electronic, Photonic and Mechanical Neuronal Interfacing. New York, NY: Springer New York; 2014. p. 71-134.

4. Schwartz AB, Cui XT, Weber DJ, Moran DW. Brain-controlled interfaces: movement restoration with neural prosthetics. Neuron. 2006; 52:205–20. [PubMed: 17015237]

5. Kipke DR, Shain W, Buzsaki G, Fetz E, Henderson JM, Hetke JF, et al. Advanced neurotechnologies for chronic neural interfaces: new horizons and clinical opportunities. J Neurosci. 2008; 28:11830–8. [PubMed: 19005048]

6. Buzsaki G, Anastassiou CA, Koch C. The origin of extracellular fields and currents--EEG, ECoG, LFP and spikes. Nat Rev Neurosci. 2012; 13:407–20. [PubMed: 22595786]

7. Robinson, TE.; Justice, JB. Microdialysis in the Neurosciences: Techniques in the Behavioral and Neural Sciences. Elsevier; 2013.

8. Davies MI, Cooper JD, Desmond SS, Lunte CE, Lunte SM. Analytical considerations for microdialysis sampling. Advanced drug delivery reviews. 2000; 45:169–88. [PubMed: 11108973]

9. Watson CJ, Venton BJ, Kennedy RT. In vivo measurements of neurotransmitters by microdialysis sampling. Analytical chemistry. 2006; 78:1391–9. [PubMed: 16570388]

10. Westerink, BH.; Cremers, TI. Handbook of microdialysis: methods, applications and perspectives. Academic Press; 2007.

11. Bellander BM, Cantais E, Enblad P, Hutchinson P, Nordstrom CH, Robertson C, et al. Consensus meeting on microdialysis in neurointensive care. Intensive Care Med. 2004; 30:2166–9. [PubMed: 15549254]

12. Bosche B, Dohmen C, Graf R, Neveling M, Staub F, Kracht L, et al. Extracellular concentrations of non-transmitter amino acids in peri-infarct tissue of patients predict malignant middle cerebral artery infarction. Stroke. 2003; 34:2908–13. [PubMed: 14631090]

13. Schlenk F, Frieler K, Nagel A, Vajkoczy P, Sarrafzadeh AS. Cerebral microdialysis for detection of bacterial meningitis in aneurysmal subarachnoid hemorrhage patients: a cohort study. Crit Care. 2009; 13:R2. [PubMed: 19154580]

14. Sakowitz OW, Stover JF, Sarrafzadeh AS, Unterberg AW, Kiening KL. Effects of mannitol bolus administration on intracranial pressure, cerebral extracellular metabolites, and tissue oxygenation in severely head-injured patients. Journal of Trauma and Acute Care Surgery. 2007; 62:292–8.

15. Sakowitz OW, Unterberg AW. Detecting and treating microvascular ischemia after subarachnoid hemorrhage. Current opinion in critical care. 2006; 12:103–11. [PubMed: 16543784]

16. Sarrafzadeh AS, Sakowitz OW, Kiening KL, Benndorf G, Lanksch WR, Unterberg AW. Bedside microdialysis: A tool to monitor cerebral metabolism in subarachnoid hemorrhage patients?*. Critical care medicine. 2002; 30:1062–70. [PubMed: 12006804]

17. Strong AJ, Boutelle MG, Vespa PM, Bullock MR, Bhatia R, Hashemi P. Treatment of critical care patients with substantial acute ischemic or traumatic brain injury. Critical care medicine. 2005; 33:2147–9. [PubMed: 16148510]

18. Strong AJ, Hartings JA, Dreier JP. Cortical spreading depression: an adverse but treatable factor in intensive care? Current opinion in critical care. 2007; 13:126–33. [PubMed: 17327732]

19. Nordstrom C-H. Cerebral energy metabolism and microdialysis in neurocritical care. Child's Nervous System. 2010; 26:465–72.

20. Obrenovitch T, Richards D, Sarna G, Symon L. Combined intracerebral microdialysis and electrophysiological recording: methodology and applications. Journal of neuroscience methods. 1993; 47:139–45. [PubMed: 8100599]

21. Dreier JP, Woitzik J, Fabricius M, Bhatia R, Major S, Drenckhahn C, et al. Delayed ischaemic neurological deficits after subarachnoid haemorrhage are associated with clusters of spreading depolarizations. Brain. 2006; 129:3224–37. [PubMed: 17067993]

22. Jaquins-Gerstl A, Michael AC. A review of the effects of FSCV and microdialysis measurements on dopamine release in the surrounding tissue. Analyst. 2015; 140:3696–708. [PubMed: 25876757]
23. Benveniste H, Diemer NH. Cellular reactions to implantation of a microdialysis tube in the rat hippocampus. Acta Neuropathol. 1987; 74:234–8. [PubMed: 3673515]
24. Clapp-Lilly KL, Roberts RC, Duffy LK, Irons KP, Hu Y, Drew KL. An ultrastructural analysis of tissue surrounding a microdialysis probe. J Neurosci Methods. 1999; 90:129–42. [PubMed: 10513596]
25. Zhou F, Zhu X, Castellani RJ, Stimmelmayr R, Perry G, Smith MA, et al. Hibernation, a model of neuroprotection. Am J Pathol. 2001; 158:2145–51. [PubMed: 11395392]
26. Hascup ER, af Bjerken S, Hascup KN, Pomerleau F, Huettl P, Stromberg I, et al. Histological studies of the effects of chronic implantation of ceramic-based microelectrode arrays and microdialysis probes in rat prefrontal cortex. Brain Res. 2009; 1291:12–20. [PubMed: 19577548]
27. Jaquins-Gerstl A, Shu Z, Zhang J, Liu Y, Weber SG, Michael AC. Effect of dexamethasone on gliosis, ischemia, and dopamine extraction during microdialysis sampling in brain tissue. Analytical Chemistry. 2011; 83:7662–7. [PubMed: 21859125]
28. Nesbitt KM, Varner EL, Jaquins-Gerstl A, Michael AC. Microdialysis in the Rat Striatum: Effects of 24 h Dexamethasone Retrodialysis on Evoked Dopamine Release and Penetration Injury. Acs Chemical Neuroscience. 2015; 6:163–73. [PubMed: 25491242]
29. Nesbitt KM, Jaquins-Gerstl A, Skoda EM, Wipf P, Michael AC. Pharmacological mitigation of tissue damage during brain microdialysis. Analytical Chemistry. 2013; 85:8173–9. [PubMed: 23927692]
30. Kozai TDY, Marzullo TC, Hooi F, Langhals NB, Majewska AK, Brown EB, et al. Reduction of neurovascular damage resulting from microelectrode insertion into the cerebral cortex using in vivo two-photon mapping. J Neural Eng. 2010; 7:046011. [PubMed: 20644246]
31. Kozai, T.; Langhals, N.; Hooi, F.; Kipke, D. Time Course of Blood Brain Barrier Disruption Due to Microelectrode Insertion into Cerebral Cortex. Annual Meeting; Pittsburgh, PA. Oct 7–10. 2009; Biomedical Engineering Society;
32. Kozai TDY, Jaquins-Gerstl A, Vazquez AL, Michael AC, Cui XT. Brain Tissue Responses to Neural Implants Impact Signal Sensitivity and Intervention Strategies. ACS Chemical Neuroscience. 2015; 6:48–67. [PubMed: 25546652]
33. Kozai TDY, Vazquez AL, Weaver CL, Kim SG, Cui XT. In vivo two photon microscopy reveals immediate microglial reaction to implantation of microelectrode through extension of processes. J Neural Eng. 2012; 9:066001. [PubMed: 23075490]
34. Kozai TDY, Li X, Bodily LM, Caparosa EM, Zenonos GA, Carlisle DL, et al. Effects of caspase-1 knockout on chronic neural recording quality and longevity: Insight into cellular and molecular mechanisms of the reactive tissue response. Biomaterials. 2014; 35:9620–34. [PubMed: 25176060]
35. Tremblay ME, Lowery RL, Majewska AK. Microglial interactions with synapses are modulated by visual experience. PLoS biology. 2010; 8:e1000527. [PubMed: 21072242]
36. Wake H, Moorhouse AJ, Jinno S, Kohsaka S, Nabekura J. Resting microglia directly monitor the functional state of synapses in vivo and determine the fate of ischemic terminals. J Neurosci. 2009; 29:3974–80. [PubMed: 19339593]
37. Nimmerjahn A, Kirchhoff F, Helmchen F. Resting microglial cells are highly dynamic surveillants of brain parenchyma in vivo. Science. 2005; 308:1314–8. [PubMed: 15831717]
38. Davalos D, Grutzendler J, Yang G, Kim JV, Zuo Y, Jung S, et al. ATP mediates rapid microglial response to local brain injury in vivo. Nature neuroscience. 2005; 8:752–8. [PubMed: 15895084]
39. Purcell EK, Seymour JP, Yandamuri S, Kipke DR. In vivo evaluation of a neural stem cell-seeded prosthesis. J Neural Eng. 2009; 6:026005. [PubMed: 19287078]
40. Kozai TDY, Eles JR, Vazquez AL, Cui XT. Two-photon imaging of chronically implanted neural electrodes: Sealing methods and new insights. Journal of Neuroscience Methods. 2016; 256:46–55. [PubMed: 26526459]
41. Biran R, Martin DC, Tresco PA. Neuronal cell loss accompanies the brain tissue response to chronically implanted silicon microelectrode arrays. Experimental Neurology. 2005; 195:115–26. [PubMed: 16045910]

42. Szarowski DH, Andersen MD, Retterer S, Spence AJ, Isaacson M, Craighead HG, et al. Brain responses to micro-machined silicon devices. Brain Res. 2003; 983:23–35. [PubMed: 12914963]
43. Kozai TDY, Gugel Z, Li X, Gilgunn PJ, Khilwani R, Ozdoganlar OB, et al. Chronic tissue response to carboxymethyl cellulose based dissolvable insertion needle for ultra-small neural probes. Biomaterials. 2014; 35:9255–68. [PubMed: 25128375]
44. Kozai TDY, Langhals NB, Patel PR, Deng X, Zhang H, Smith KL, et al. Ultrasmall implantable composite microelectrodes with bioactive surfaces for chronic neural interfaces. Nat Mater. 2012; 11:1065–73. [PubMed: 23142839]
45. Roitbak T, Sykova E. Diffusion barriers evoked in the rat cortex by reactive astrogliosis. Glia. 1999; 28:40–8. [PubMed: 10498821]
46. Jaquins-Gerstl A, Michael AC. Comparison of the brain penetration injury associated with microdialysis and voltammetry. Journal of Neuroscience Methods. 2009; 183:127–35. [PubMed: 19559724]
47. Williams JC, Hippensteel JA, Dilgen J, Shain W, Kipke DR. Complex impedance spectroscopy for monitoring tissue responses to inserted neural implants. J Neural Eng. 2007; 4:410–23. [PubMed: 18057508]
48. Karumbaiah L, Norman SE, Rajan NB, Anand S, Saxena T, Betancur M, et al. The upregulation of specific interleukin (IL) receptor antagonists and paradoxical enhancement of neuronal apoptosis due to electrode induced strain and brain micromotion. Biomaterials. 2012; 33:5983–96. [PubMed: 22681976]
49. Holson RR, Gazzara RA, Gough B. Declines in stimulated striatal dopamine release over the first 32 h following microdialysis probe insertion: generalization across releasing mechanisms. Brain Research. 1998; 808:182–9. [PubMed: 9767162]
50. Holson RR, Bowyer JF, Clausing P, Gough B. Methamphetamine-stimulated striatal dopamine release declines rapidly over time following microdialysis probe insertion. Brain Research. 1996; 739:301–7. [PubMed: 8955951]
51. Patel PR, Na K, Zhang H, Kozai TDY, Kotov NA, Yoon E, et al. Insertion of linear 8.4 μm diameter 16 channel carbon fiber electrode arrays for single unit recordings. Journal of Neural Engineering. 2015; 12:046009. [PubMed: 26035638]
52. Seymour JP, Kipke DR. Neural probe design for reduced tissue encapsulation in CNS. Biomaterials. 2007; 28:3594–607. [PubMed: 17517431]
53. Seymour JP, Langhals NB, Anderson DJ, Kipke DR. Novel multi-sided, microelectrode arrays for implantable neural applications. Biomed Microdevices. 2011
54. Kozai TD, Li X, Bodily LM, Caparosa EM, Zenonos GA, Carlisle DL, et al. Effects of caspase-1 knockout on chronic neural recording quality and longevity: Insight into cellular and molecular mechanisms of the reactive tissue response. Biomaterials. 2014; 35:9620–34. [PubMed: 25176060]
55. Kozai TD, Langhals NB, Patel PR, Deng X, Zhang H, Smith KL, et al. Ultrasmall implantable composite microelectrodes with bioactive surfaces for chronic neural interfaces. Nat Mater. 2012; 11:1065–73. [PubMed: 23142839]
56. Kozai TDY, Catt K, Li X, Gugel ZV, Olafsson VT, Vazquez AL, et al. Mechanical failure modes of chronically implanted planar silicon-based neural probes for laminar recording. Biomaterials. 2015; 37:25–39. [PubMed: 25453935]
57. Gilgunn, PJ.; Khilwani, R.; Kozai, TDY.; Weber, DJ.; Cui, XT.; Erdos, G., et al. An ultra-compliant, scalable neural probe with molded biodissolvable delivery vehicle. Micro Electro Mechanical Systems (MEMS); 2012 IEEE 25th International Conference on; 2012. p. 56-9.
58. Harris JP, Capadona JR, Miller RH, Healy BC, Shanmuganathan K, Rowan SJ, et al. Mechanically adaptive intracortical implants improve the proximity of neuronal cell bodies. J Neural Eng. 2011; 8:066011. [PubMed: 22049097]
59. Ware T, Simon D, Liu C, Musa T, Vasudevan S, Sloan A, et al. Thiol-ene/acrylate substrates for softening intracortical electrodes. J Biomed Mater Res B Appl Biomater. 2014; 102:1–11. [PubMed: 23666562]
60. Kozai TDY, Kipke DR. Insertion shuttle with carboxyl terminated self-assembled monolayer coatings for implanting flexible polymer neural probes in the brain. J Neurosci Methods. 2009; 184:199–205. [PubMed: 19666051]

61. Kolarcik CL, Luebben SD, Sapp SA, Hanner J, Snyder N, Kozai TD, et al. Elastomeric and soft conducting microwires for implantable neural interfaces. Soft matter. 2015; 11(2015):4847–61. [PubMed: 25993261]
62. Cui X, Martin DC. Electrochemical deposition and characterization of poly (3, 4-ethylenedioxythiophene) on neural microelectrode arrays. Sensors and Actuators B: Chemical. 2003; 89:92–102.
63. Cui X, Martin DC. Fuzzy gold electrodes for lowering impedance and improving adhesion with electrodeposited conducting polymer films. Sensors and Actuators A: Physical. 2003; 103:384–94.
64. Cui X, Hetke JF, Wiler JA, Anderson DJ, Martin DC. Electrochemical deposition and characterization of conducting polymer polypyrrole/PSS on multichannel neural probes. Sensors and Actuators A: Physical. 2001; 93:8–18.
65. Kozai TDY, Catt K, Du Z, Kyounghwan N, Srivannavit O, Haque RM, et al. Chronic in vivo evaluation of PEDOT/CNT for stable neural recordings. IEEE Trans Biomed Eng. 2015; 63(2016): 111–119.10.1109/TBME.2015.2445713 [PubMed: 26087481]
66. Kolarcik CL, Catt K, Rost E, Albrecht IN, Bourbeau D, Du Z, et al. Evaluation of poly(3,4-ethylenedioxythiophene)/carbon nanotube neural electrode coatings for stimulation in the dorsal root ganglion. J Neural Eng. 2015; 12:016008. [PubMed: 25485675]
67. Bjornsson CS, Oh SJ, Al-Kofahi YA, Lim YJ, Smith KL, Turner JN, et al. Effects of insertion conditions on tissue strain and vascular damage during neuroprosthetic device insertion. J Neural Eng. 2006; 3:196–207. [PubMed: 16921203]
68. Johnson MD, Kao OE, Kipke DR. Spatiotemporal pH dynamics following insertion of neural microelectrode arrays. J Neurosci Methods. 2007; 160:276–87. [PubMed: 17084461]
69. Kolarcik CL, Bourbeau D, Azemi E, Rost E, Zhang L, Lagenaur CF, et al. In vivo effects of L1 coating on inflammation and neuronal health at the electrode-tissue interface in rat spinal cord and dorsal root ganglion. Acta Biomater. 2012; 8:3561–75. [PubMed: 22750248]
70. Azemi E, Lagenaur CF, Cui XT. The surface immobilization of the neural adhesion molecule L1 on neural probes and its effect on neuronal density and gliosis at the probe/tissue interface. Biomaterials. 2011; 32:681–92. [PubMed: 20933270]
71. Zhong Y, Bellamkonda RV. Controlled release of anti-inflammatory agent [alpha]-MSH from neural implants. Journal of Controlled Release. 2005; 106:309–18. [PubMed: 15978692]
72. Hue CD, Cho FS, Cao S, Dale Bass CR, Meaney DF, Morrison B Iii. Dexamethasone potentiates in vitro blood-brain barrier recovery after primary blast injury by glucocorticoid receptor-mediated upregulation of ZO-1 tight junction protein. J Cereb Blood Flow Metab. 2015; 35:1191–8. [PubMed: 25757751]
73. Luo X, Matranga C, Tan S, Alba N, Cui XT. Carbon nanotube nanoreservior for controlled release of anti-inflammatory dexamethasone. Biomaterials. 2011; 32:6316–23. [PubMed: 21636128]
74. Leprince L, Dogimont A, Magnin D, Demoustier-Champagne S. Dexamethasone electrically controlled release from polypyrrole-coated nanostructured electrodes. Journal of materials science Materials in medicine. 2010; 21:925–30. [PubMed: 20143134]
75. Zhong Y, Bellamkonda RV. Dexamethasone-coated neural probes elicit attenuated inflammatory response and neuronal loss compared to uncoated neural probes. Brain research. 2007; 1148:15–27. [PubMed: 17376408]
76. Wadhwa R, Lagenaur CF, Cui XT. Electrochemically controlled release of dexamethasone from conducting polymer polypyrrole coated electrode. J Control Release. 2006; 110:531–41. [PubMed: 16360955]
77. Kim DH, Martin DC. Sustained release of dexamethasone from hydrophilic matrices using PLGA nanoparticles for neural drug delivery. Biomaterials. 2006; 27:3031–7. [PubMed: 16443270]
78. Spataro L, Dilgen J, Retterer S, Spence AJ, Isaacson M, Turner JN, et al. Dexamethasone treatment reduces astroglia responses to inserted neuroprosthetic devices in rat neocortex. Experimental Neurology. 2005; 194:289–300. [PubMed: 16022859]
79. Shain W, Spataro L, Dilgen J, Haverstick K, Retterer S, Isaacson M, et al. Controlling cellular reactive responses around neural prosthetic devices using peripheral and local intervention strategies. IEEE Trans Neural Syst Rehabil Eng. 2003; 11:186–8. [PubMed: 12899270]

80. Williams GA, Haller JA, Kuppermann BD, Blumenkranz MS, Weinberg DV, Chou C, et al. Dexamethasone posterior-segment drug delivery system in the treatment of macular edema resulting from uveitis or Irvine-Gass syndrome. American journal of ophthalmology. 2009; 147:1048–54. 54 e1–2. [PubMed: 19268890]
81. Chang A, Eastwood H, Sly D, James D, Richardson R, O'Leary S. Factors influencing the efficacy of round window dexamethasone protection of residual hearing post-cochlear implant surgery. Hearing research. 2009; 255:67–72. [PubMed: 19539739]
82. Luo X, Cui XT. Electrochemical deposition of conducting polymer coatings on magnesium surfaces in ionic liquid. Acta Biomater. 2011; 7:441–6. [PubMed: 20832505]
83. Mitala CM, Wang Y, Borland LM, Jung M, Shand S, Watkins S, et al. Impact of microdialysis probes on vasculature and dopamine in the rat striatum: a combined fluorescence and voltammetric study. Journal of Neuroscience Methods. 2008; 174:177–85. [PubMed: 18674561]
84. Munk A, Guyre PM, Holbrook NJ. Physiological functions of glucocorticoids in stress and their relation to pharmacological actions*. Endocrine reviews. 1984; 5:25–44. [PubMed: 6368214]
85. Makino S, Hashimoto K, Gold PW. Multiple feedback mechanisms activating corticotropin-releasing hormone system in the brain during stress. Pharmacology, biochemistry, and behavior. 2002; 73:147–58.
86. Reichardt HM, Tuckermann JP, Gottlicher M, Vujic M, Weih F, Angel P, et al. Repression of inflammatory responses in the absence of DNA binding by the glucocorticoid receptor. The EMBO journal. 2001; 20:7168–73. [PubMed: 11742993]
87. Galicich J, French LA. Use of dexamethasone in the treatment of cerebral edema resulting from brain tumors and brain surgery. American practitioner and digest of treatment. 1961; 12:169–74. [PubMed: 13703073]
88. Avery GB, Fletcher AB, Kaplan M, Brudno DS. Controlled trial of dexamethasone in respirator-dependent infants with bronchopulmonary dysplasia. Pediatrics. 1985; 75:106–11. [PubMed: 3880879]
89. Bernini JC, Rogers ZR, Sandler ES, Reisch JS, Quinn CT, Buchanan GR. Beneficial effect of intravenous dexamethasone in children with mild to moderately severe acute chest syndrome complicating sickle cell disease. Blood. 1998; 92:3082–9. [PubMed: 9787142]
90. Lukins MB, Manninen PH. Hyperglycemia in patients administered dexamethasone for craniotomy. Anesthesia and analgesia. 2005; 100:1129–33. [PubMed: 15781533]
91. Markovic A, Todorovic L. Effectiveness of dexamethasone and low-power laser in minimizing oedema after third molar surgery: a clinical trial. International journal of oral and maxillofacial surgery. 2007; 36:226–9. [PubMed: 17157479]
92. Matyszak MK, Perry VH. The potential role of dendritic cells in immune-mediated inflammatory diseases in the central nervous system. Neuroscience. 1996; 74:599–608. [PubMed: 8865208]
93. Yeh TF, Torre JA, Rastogi A, Anyebuno MA, Pildes RS. Early postnatal dexamethasone therapy in premature infants with severe respiratory distress syndrome: a double-blind, controlled study. The Journal of pediatrics. 1990; 117:273–82. [PubMed: 2199642]
94. Wang DL, Wung BS, Shyy YJ, Lin CF, Chao YJ, Usami S, et al. Mechanical strain induces monocyte chemotactic protein-1 gene expression in endothelial cells. Effects of mechanical strain on monocyte adhesion to endothelial cells. Circulation research. 1995; 77:294–302. [PubMed: 7614716]
95. Iqbal J, Zaidi M. Molecular regulation of mechanotransduction. Biochemical and biophysical research communications. 2005; 328:751–5. [PubMed: 15694410]
96. Willis D, Li KW, Zheng JQ, Chang JH, Smit AB, Kelly T, et al. Differential transport and local translation of cytoskeletal, injury-response, and neurodegeneration protein mRNAs in axons. J Neurosci. 2005; 25:778–91. [PubMed: 15673657]
97. Calderwood SK, Mambula SS, Gray PJ Jr. Extracellular heat shock proteins in cell signaling and immunity. Annals of the New York Academy of Sciences. 2007; 1113:28–39. [PubMed: 17978280]
98. Kountz DS, Clark CL. Safely withdrawing patients from chronic glucocorticoid therapy. American family physician. 1997; 55:521–5. 9–30. [PubMed: 9054221]

99. Greenspan, FS.; Gardner, DG.; Shoback, D. Basic & clinical endocrinology. Appleton & Lange; Stamford, CT: 1997.

100. Hempen C, Weiss E, Hess CF. Dexamethasone treatment in patients with brain metastases and primary brain tumors: do the benefits outweigh the side-effects? Supportive care in cancer. 2002; 10:322–8. [PubMed: 12029432]

101. Koehler P. Use of corticosteroids in neuro-oncology. Anti-cancer drugs. 1995; 6:19–33. [PubMed: 7756680]

102. Raison CL, Miller AH. When not enough is too much: the role of insufficient glucocorticoid signaling in the pathophysiology of stress-related disorders. American Journal of Psychiatry. 2003; 160:1554–65. [PubMed: 12944327]

103. Chrousos GP. Stress and disorders of the stress system. Nature reviews Endocrinology. 2009; 5:374–81.

104. McEwen BS. Physiology and neurobiology of stress and adaptation: central role of the brain. Physiological reviews. 2007; 87:873–904. [PubMed: 17615391]

105. Kozai TDY, Jaquins-Gerstl AS, Vazquez AL, Michael AC, Cui XT. Brain Tissue Responses to Neural Implants Impact Signal Sensitivity and Intervention Strategies. ACS Chemical Neuroscience. 2015; 6(2015):48–67. [PubMed: 25546652]

106. Rousche PJ, Normann RA. Chronic recording capability of the Utah Intracortical Electrode Array in cat sensory cortex. J Neurosci Methods. 1998; 82:1–15. [PubMed: 10223510]

107. Williams JC, Rennaker RL, Kipke DR. Long-term neural recording characteristics of wire microelectrode arrays implanted in cerebral cortex. Brain Res Brain Res Protoc. 1999; 4:303–13. [PubMed: 10592339]

108. Varner EL, Jaquins-Gerstl A, Michael AC. Enhanced Intracranial Microdialysis by Elimination of the Traumatic Penetration Injury at the Probe Track. ACS Chem Neurosci. 2016 Submitted.

109. Alba NA, Du Z, Catt K, Kozai TDY, Cui XT. In vivo electrochemical analysis of a PEDOT/MWCNT neural electrode. Biosensors. 2015; 5:618–648. [PubMed: 26473938]

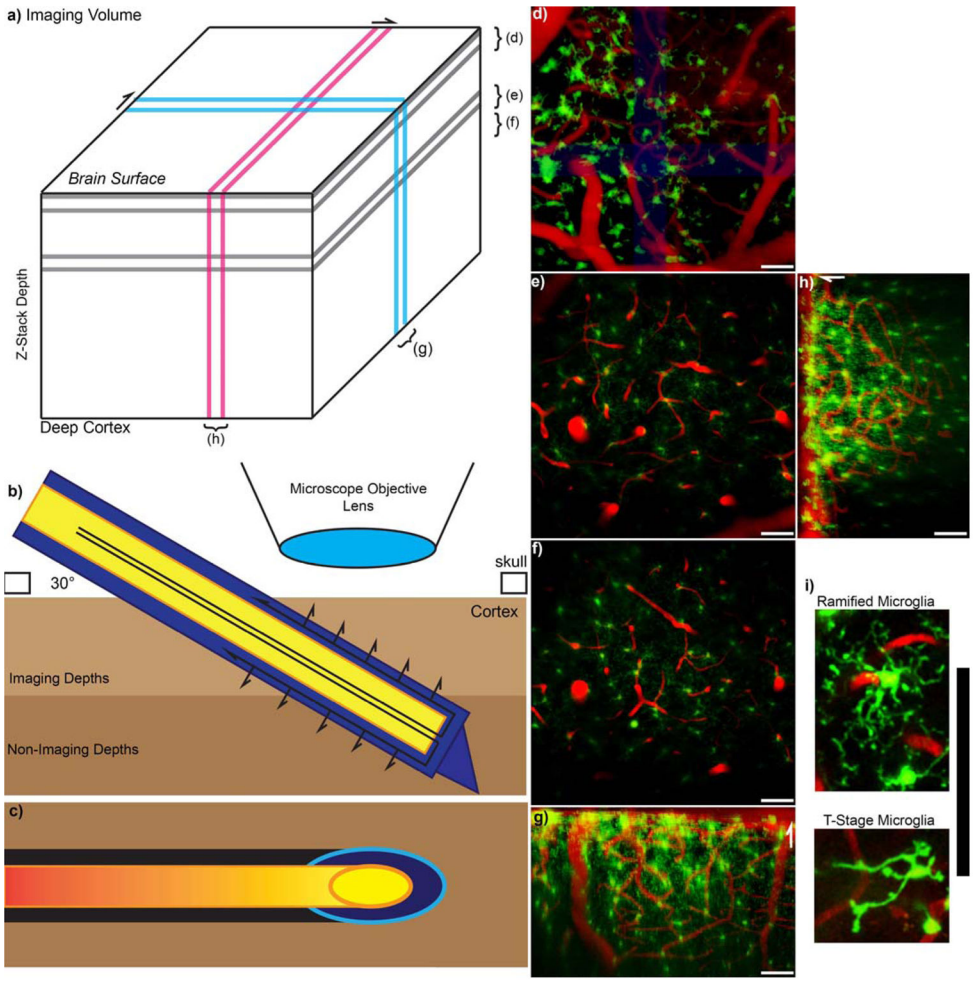

Figure 1. Experimental Setup

a) Model Z-stack imaging volume with Two Photon Microscopy. Brackets for d–f indicate z-projections that are parallel to the skull or surface of the brain, while g and h indicate y-projection and x-projection 3D reconstruction, respectively. **b)** Schematic of the experimental setup. The outer membrane of the microdialysis probe is indicated in blue, while the inner fused silica tube is indicated in yellow. The probe is inserted at a 30-degree angle to prevent collision with the microscope objective. Arrows indicate direction of perfusion flow and passive diffusion of perfusate. **c)** Because the microdialysis probe is inserted at an angle, the footprint of the probe in each acquired xy-image is an ellipse as indicated by the cyan and orange. Black and red highlight the optic shadow created by the microdialysis probe above. **d)** The top 50 microns at the surface of the brain is covered with large surface macrophages. **e–f)** 100–150 μm and 150–200 μm Z-projections show ramified (normal) microglia with radially extended processes. (d–f) are parallel to the skull. **g–h)** 100 μm thick 3D reconstruction side view. White arrows point towards surface of the brain. **i)** Zoomed in image of a ramified (R-stage) microglia and transition stage (T-stage) microglia. All scale = 100 μm.

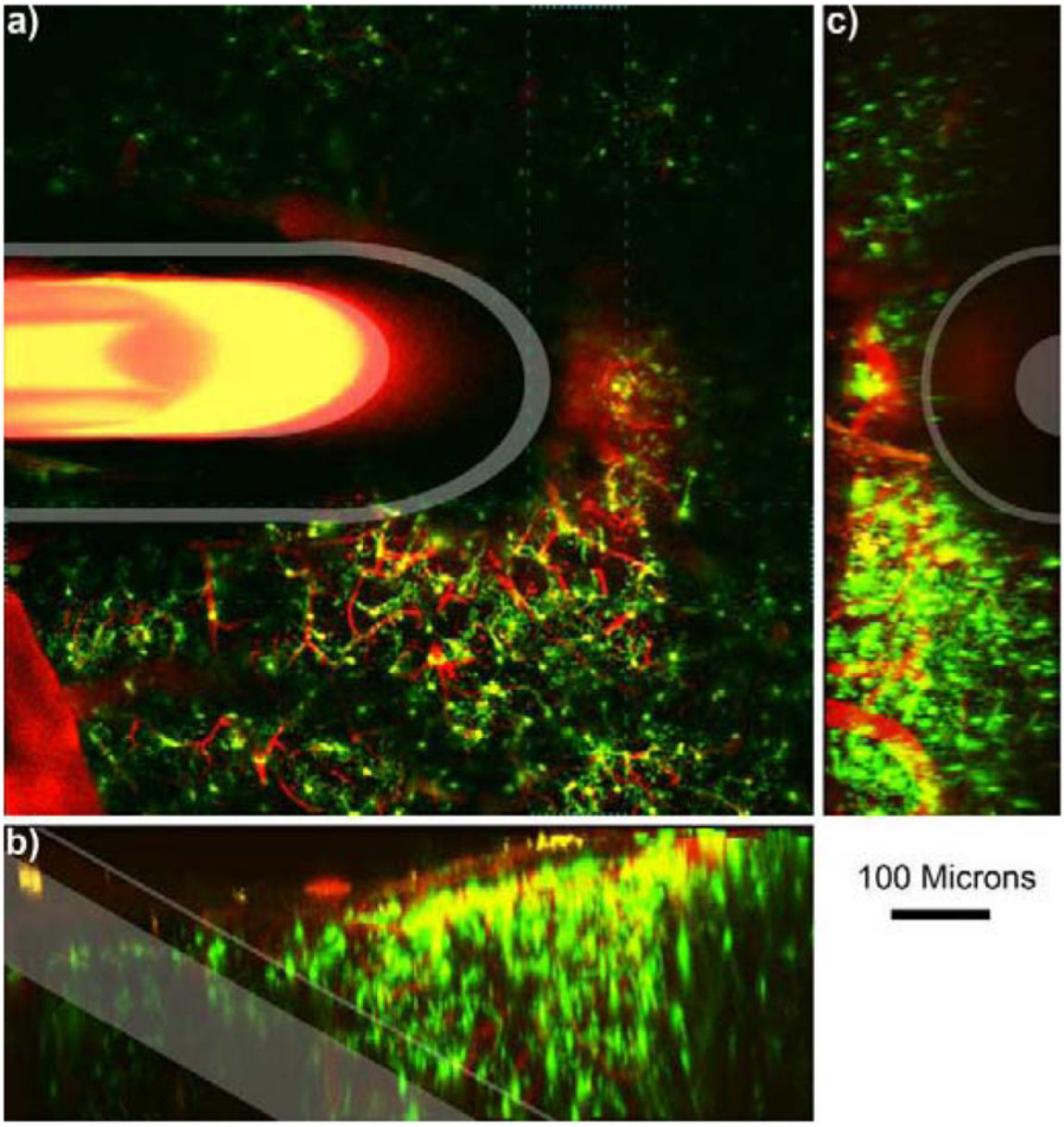

Figure 2.

Microdialysis Probe *in vivo* into the cortex.

a) 100 μm thick Z-projection of a microdialysis probe implanted into the tissue. The image is parallel to the skull. Outer membrane and inner fused silica tube is highlighted in white. Bleeding can be identified near the top right of the probe where iron in the blood quenches fluorescence (indicated by *). Cyan dashed line indicates the volume for 3D reconstruction of b–c. **b)** Side view 3D reconstruction of microdialysis probe. Surface of the brain is the top of (b). **c)** 3D reconstruction of the tissue rotated such that the probe is projecting out of the image. Surface of the brain is to the left of (c). Scale = 100 μm.

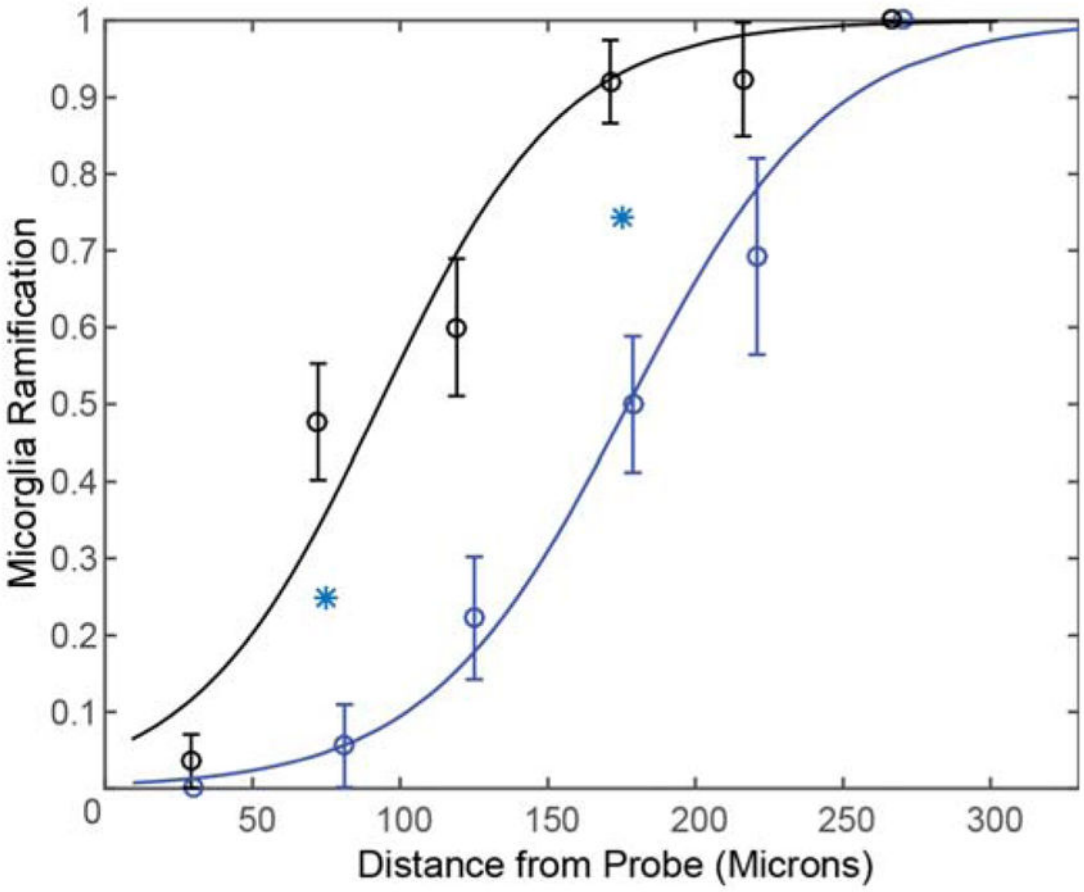

Figure 3.

Dex reduces Microglial Activation. Curves characterize microglia ramification versus the distance from the probe. Index = 1 represents all microglial cells being ramified, while index = 0 represents all microglial cells being activated around Dex (black, n=8) and aCSF (blue, n=8) perfused microdialysis probes. Line is the best fit logarithmic binomial generalized linear regression curve. Cyan stars indicate significant difference (p<0.05).

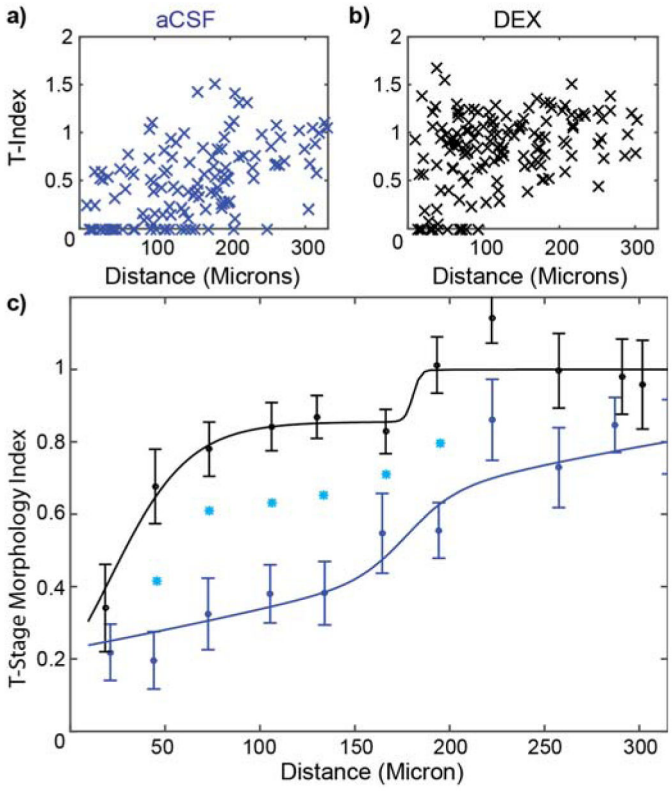

Figure 4.

Dex Significantly Reduces Microglial T-Stage Morphology Activation. T-stage morphology index where 1 is the ramified state and 0 is the transitional stage of activated microglia. T-index of individual microglial cells around aCSF (a: blue, n=8) and Dex (b: black, n=8) perfused microdialysis probes prior to binning. C) 30 μm binned data with curve fitting. Cyan stars indicate significant difference (p<0.05).

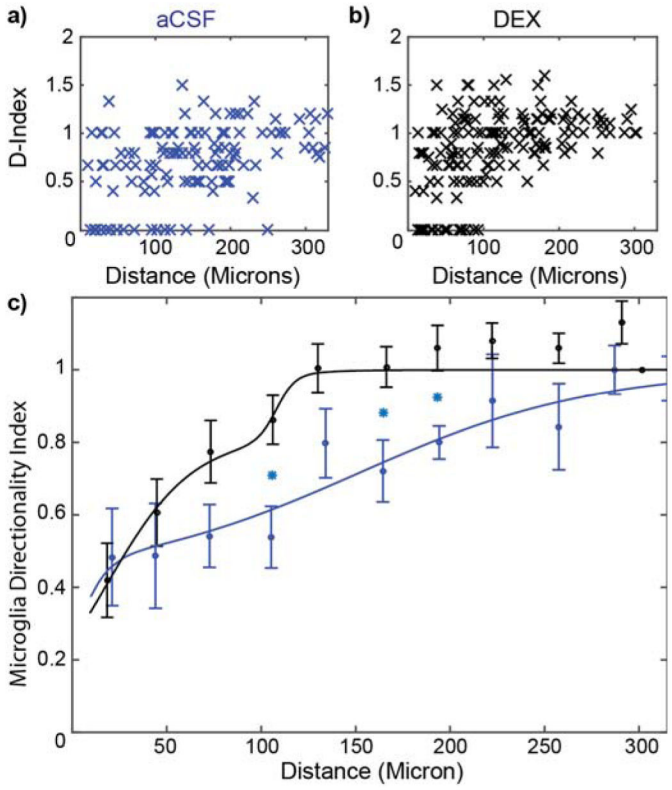

Figure 5.

Dex Significantly Reduces Microglial Directionality Polarization. D-stage morphology index where 1 is the ramified state and 0 is the transitional stage of activated microglia. D-index of individual microglial cells around aCSF (a: blue, n=8) and Dex (b: black, n=8) perfused microdialysis probes prior to binning. C) 30 μm binned data with curve fitting. Cyan stars indicate significant difference (p<0.05).

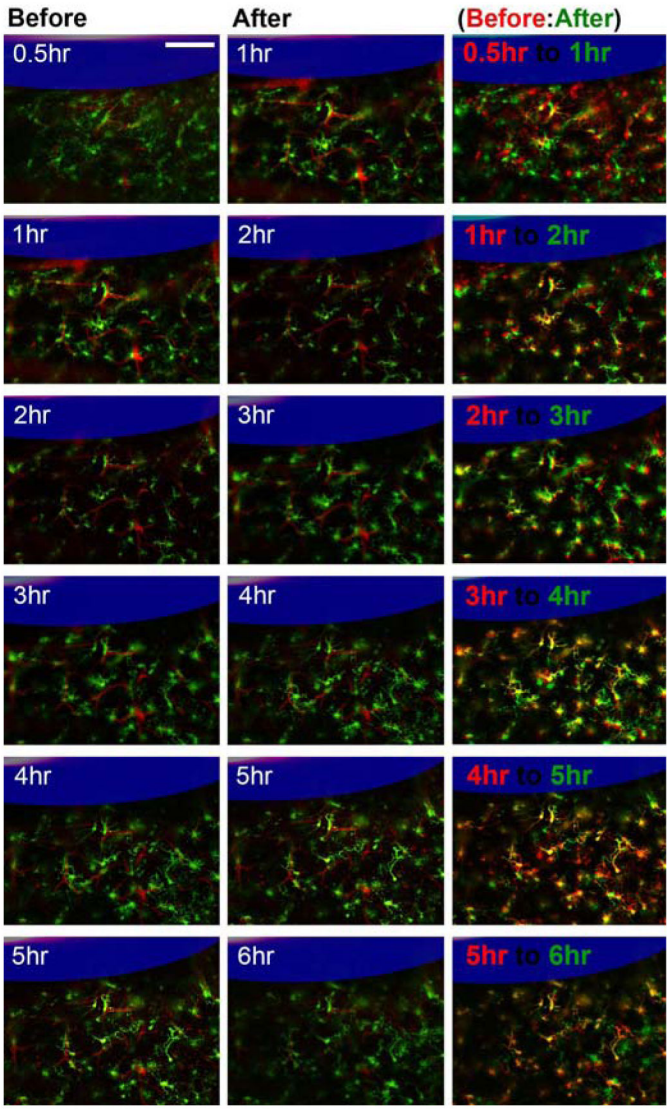

Figure 6.

Dynamic microglia reaction around aCSF perfused microdialysis from 0.5 hr to 6 hr. Microdialysis probe is outlined in blue. White numbers label static time points, red are landmark blood vessels, and green is microglia. Retraction of processes can be identified as decrease of green pixels and increase in black pixels from the first to second column. Red and green labeled panels on the right show overlap of the two time points (earlier time point in red and later time point in green: retraced processes (green), extended processes (red)). In these panels, yellow highlight common features while red and green show microglia differences between the two time points. Scale = 100 μm.

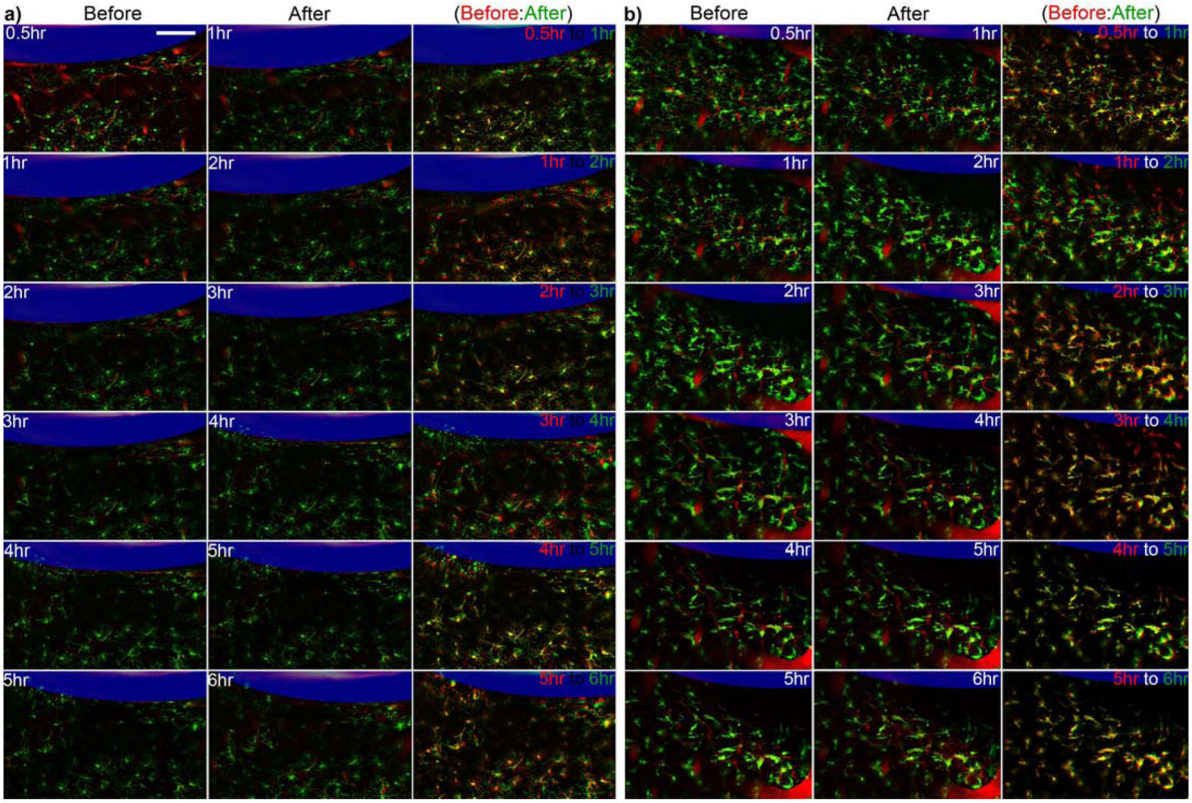

Figure 7.

Dynamic microglia reaction around Dex perfused microdialysis from 0.5 hr to 6 hr. **a)** Typical microglial reaction pattern. **b)** Rare microglia reaction pattern. Microdialysis probe is outlined in blue. Retraction of processes can be identified as decrease of green pixels and increase in black pixels from the first to second column. White numbers label static time points where red are landmark blood vessels and green is microglia. Red and green labeled panels show microglia differences between an earlier time point (red) and later time point (green) (retraced processes (green), extended processes (red)). Yellow highlight common features. Scale = 100 μm.

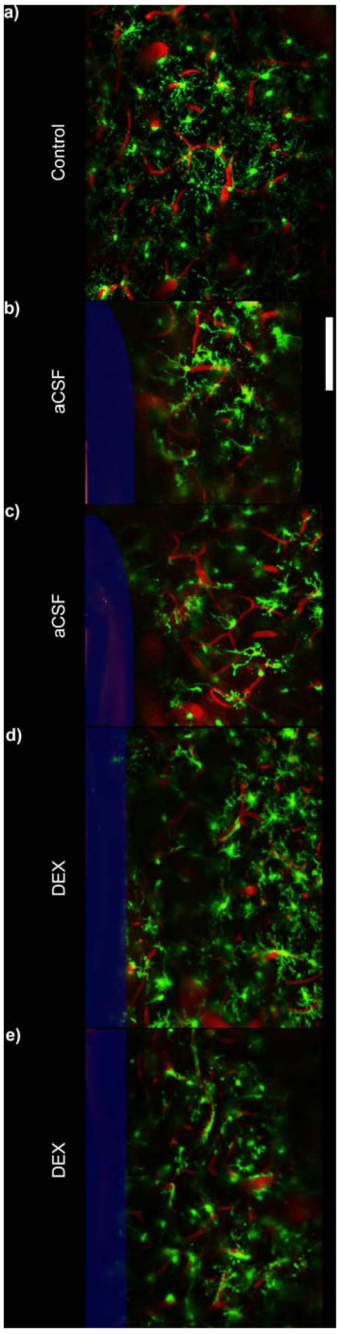

Figure 8.

Qualitative Morphological Examination (25 μm thick Z-projections). a) Microglia in non-implanted control tissue shows extended radial processes. b–c) Microglial cells around aCSF perfused microdialysis probes show a reduced number of processes that are extended towards the probe surface when compared to previous silicon study [33]. d) Microglia around Dex perfused microdialysis probes generally maintains greater level of radially extended processes. However, these processes typically have thicker basal processes and increased apical processes giving a bushier appearance when compared to ramified control

(a). e) In one example, microglial cells appeared more amoeboid with substantially reduced number of processes. While the number of processes encapsulating the probe is greatly reduced, the morphology of these cells appear very differently from *a*–*d*. Note: e is the same probe and Dex concentration as *d* (other side of the probe). Microdialysis probe is outlined in blue. Scale = 100 μm.

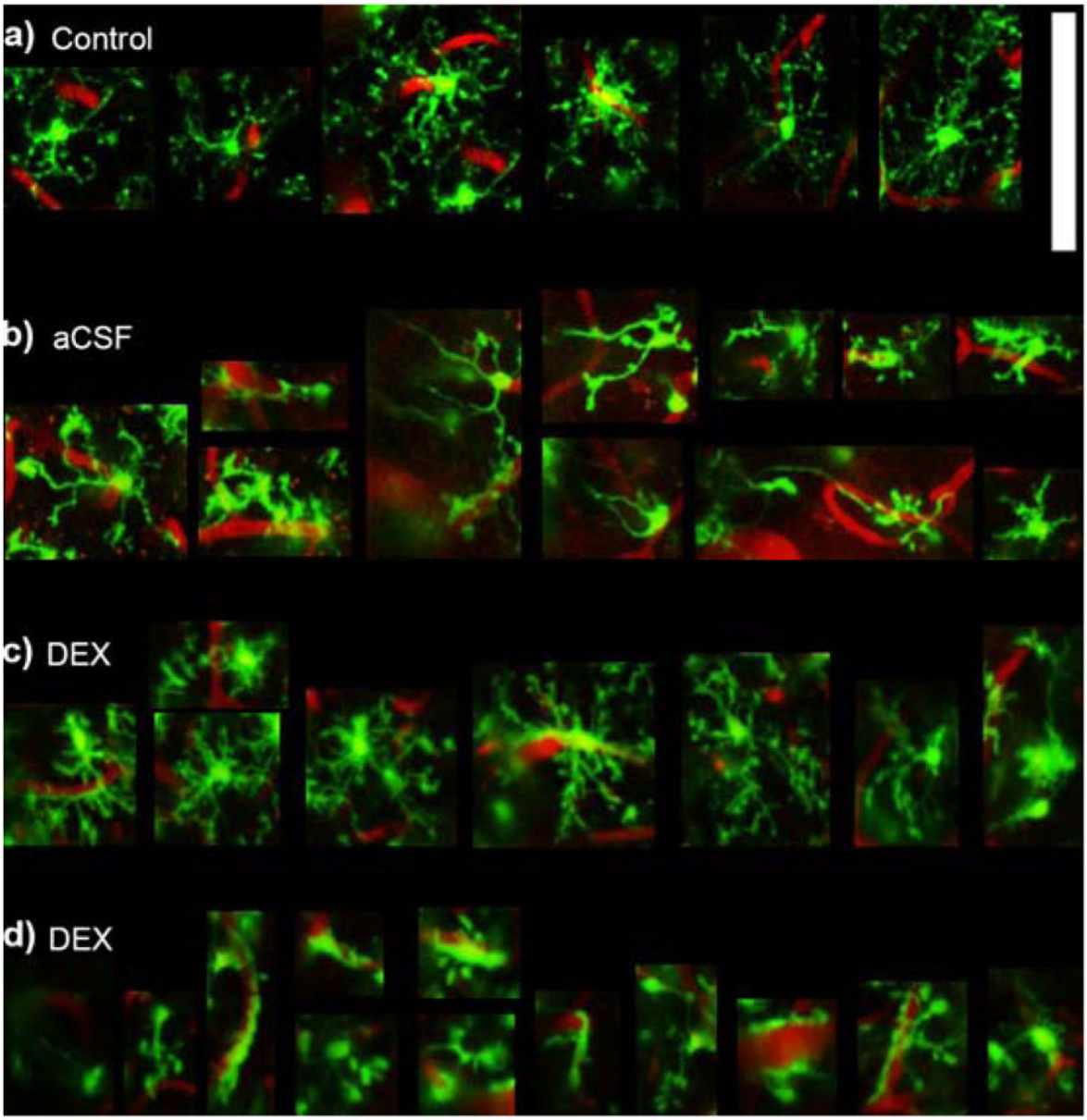

Figure 9.

Qualitative Microglial Morphology. Zoomed in images of cells from Figure 8. a) An example of ramified microglia showing thin radially expanded morphology. b) Activated microglia around aCSF perfused microdialysis probes showing reduced number of basal and apical processes and a few elongated processes towards the implant. c) Typical microglia around Dex perfused microdialysis probes show radially projected processes similar to ramified microglia, however, the processes appear thicker with increased short apical processes giving it a “bushier” morphology. d) In one instance around a Dex perfused microdialysis probe, microglia show substantially reduced number of processes and greater encapsulation of blood vessels. Note: *d* is the same animal, Dex concentration, and probe as (*c*) (other side of the probe). Scale = 100 μm.

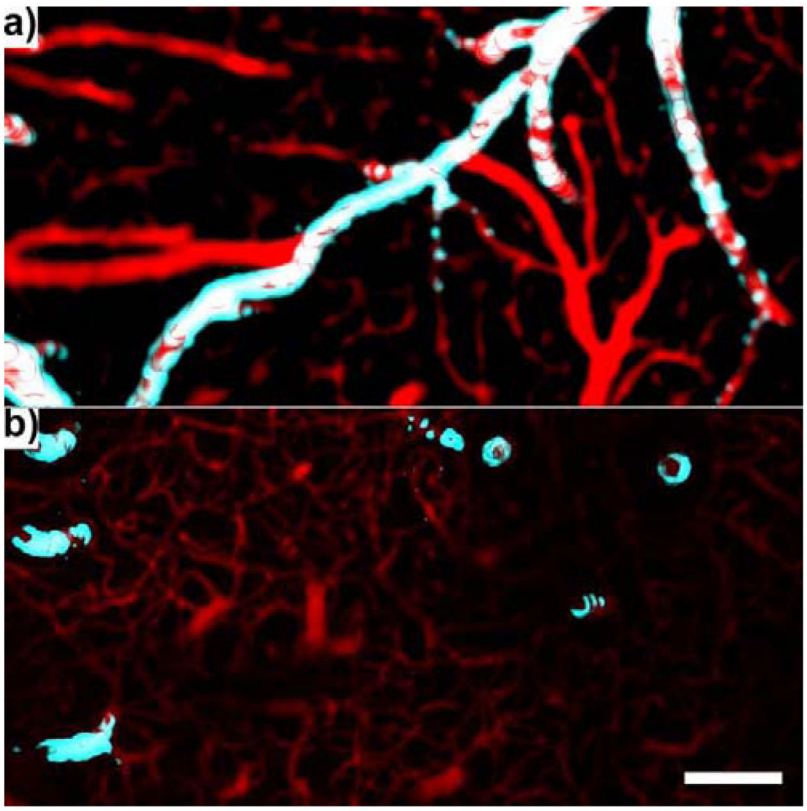

Figure 10.

Arteries and Veins. a) Surface vasculature. b) intracortical vasculature below the surface of the brain up to a depth of ~500 μm. Veins/capillaries = red. Large arteries (C57BL/6-Tg(CAG-EGFP)1Osb/J) = cyan. Scale = 100 μm.

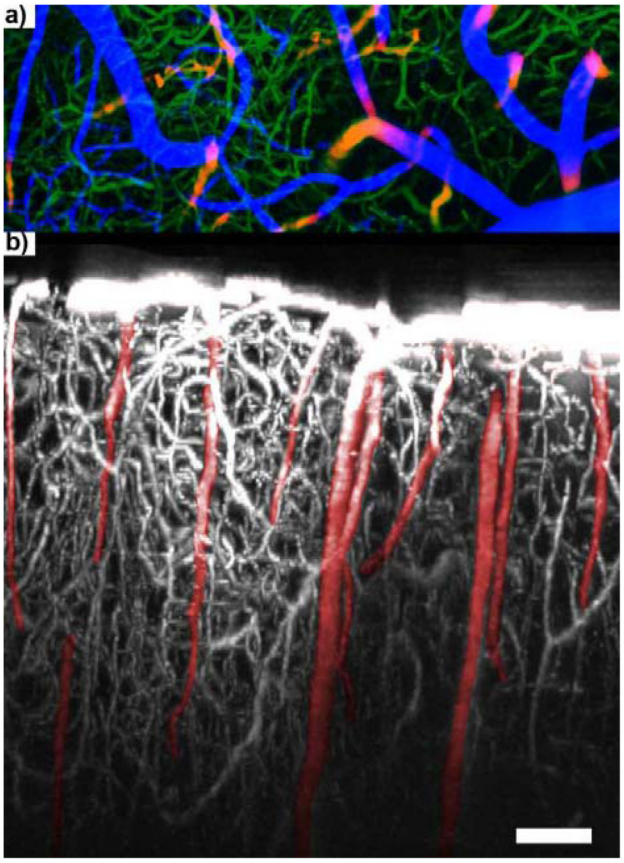

Figure 11.

950 μm In Vivo 3D BBB Map. a) “Visible” surface vessels (blue), “Invisible” intra-cortical small capillaries (green), “Invisible” major arteries and veins (red/yellow). b) Side view 3D reconstruction of BBB (white) and “Invisible” major arteries and veins (red). Arteries (A) have fewer capillaries around than veins (V), since the blood oxygenation level is generally high enough that it does not need capillaries to perfuse nearby tissue. Scale = 100 μm. Adapted) with permission from [32]. Copyright 2015 American Chemical Society.